

**SSC-165**

**Local Yielding and Extension  
of a  
Crack Under Plane Stress**

by

**G. T. HAHN**

and

**A. R. ROSENFELD**

**SHIP STRUCTURE COMMITTEE**

# SHIP STRUCTURE COMMITTEE

## MEMBER AGENCIES:

BUREAU OF SHIPS, DEPT. OF NAVY  
MILITARY SEA TRANSPORTATION SERVICE, DEPT. OF NAVY  
UNITED STATES COAST GUARD, TREASURY DEPT  
MARITIME ADMINISTRATION, DEPT. OF COMMERCE  
AMERICAN BUREAU OF SHIPPING

## ADDRESS CORRESPONDENCE TO:

SECRETARY  
SHIP STRUCTURE COMMITTEE  
U. S. COAST GUARD HEADQUARTERS  
WASHINGTON 25, D. C.

December 1964

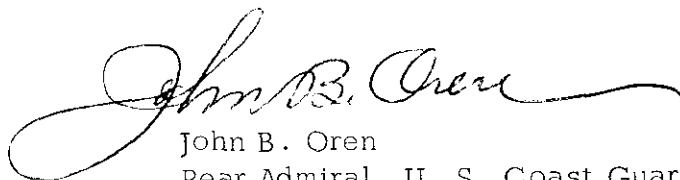
Dear Sir:

As part of its research effort in the field of brittle fracture, the Ship Structure Committee is sponsoring at Battelle Memorial Institute an experimental study of localized yielding around a notch. Concurrently at Battelle, the American Gas Association is sponsoring research concerned with crack propagation in steels. As part of the latter program, a theoretical model of a crack under stress has been developed. Since the theoretical and experimental studies are complementary, the results have been combined in this First Combined Progress Report, SSC-165, entitled Local Yielding and Extension of a Crack under Plane Stress, by G. T. Hahn and A. R. Rosenfield. The Ship Structure Committee is grateful to the American Gas Association for permission to publish the results jointly.

The experimental portion of this project has been conducted under the advisory guidance of the National Academy of Sciences-National Research Council, utilizing its Ship Hull Research Committee.

This report is being distributed to individuals and groups associated with or interested in the work of the Ship Structure Committee. Please submit any comments that you may have to the Secretary, Ship Structure Committee.

Sincerely yours,



John B. Oren  
Rear Admiral, U. S. Coast Guard  
Chairman, Ship Structure Committee

SSC-165

Combined Progress Report

of

NG 18 Research  
"Fundamentals of Crack  
Propagation Resistance"

to

American Gas Association

Project SR-164  
"Local Strain Measure-  
ment"

to

Ship Structure Committee  
(BuShips Contract NObs-88348)

LOCAL YIELDING AND EXTENSION  
OF A CRACK UNDER PLANE STRESS

by

G. T. Hahn and A. R. Rosenfield  
Battelle Memorial Institute  
Columbus, Ohio

Washington, D. C.  
National Academy of Sciences-National Research Council  
December 1964

## ABSTRACT

The size of locally yielded regions, the stress distribution, and displacements attending a crack in tension under plane stress have been calculated by extending the work of Dugdale and others. Methods have been developed to take work hardening and unloading into account. The displacements and plastic-zone sizes measured in edge-slotted silicon steel coupons are found to be in agreement with calculations. Conditions under which plane stress or plane strain are dominant in these edge-slotted specimens have also been determined. Finally, Irwin's fracture-toughness parameter and the conditions for crack extension are formulated in terms of basic material parameters consistent with experiment.

## CONTENTS

	<u>Page</u>
Introduction . . . . .	1
Properties of the DM Model . . . . .	1
Experimental Procedure . . . . .	5
Experimental Results . . . . .	7
Implications for Fracture . . . . .	10
Conclusions . . . . .	12
Acknowledgments . . . . .	12
References . . . . .	12
Appendix . . . . .	14

NATIONAL ACADEMY OF SCIENCES-NATIONAL RESEARCH COUNCIL

Division of Engineering & Industrial Research

SR-164 Project Advisory Committee

"Local Strain Measurement"

for the

Ship Hull Research Committee

Chairman:

J. J. Gilman  
University of Illinois

Members:

Maxwell Gensamer  
Columbia University

F. A. McClintock  
Massachusetts Institute of Technology

T. L. Johnston  
Ford Motor Company

INTRODUCTION

Progress in understanding fracture has been handicapped by the fragmentary picture of stress and strain in front of a crack. Experimental measurements have proven difficult. The elastic-stress-field solution of Inglis<sup>1</sup> or Irwin<sup>2</sup> are not valid close to and within the very important yielded region generated at the crack tip. The Irwin<sup>2</sup> and Wells<sup>3</sup> treatment, which does take yielding into account, is a reasonable approximation only when the yielded region is small relative to the crack length. At the same time, the quasi-rigorous solutions of elastic-plastic behavior<sup>4-6</sup> are complex and unwieldy; so far, practically no information on the stress and strain within the yielded zone attending a crack in tension has been developed in this way. Thus, it may be useful to compromise some rigor for a simpler tractable approach, particularly to deal with added complications, such as work hardening and rate-sensitive flow. For example, Hult and McClintock's<sup>7</sup> solution for a notch subjected to torsion, a case which is easier to treat, has shed useful light on the situation in tension.<sup>8, 9</sup> Knott and Cottrell<sup>10</sup> were able to exploit the idealized slip band model of a crack under pure shear, developed by Bilby, Cottrell, and Swinden,<sup>11</sup> in their study of notched bend specimens.

This paper extends the model of a crack in tension under plane stress developed by Dugdale,<sup>1,2</sup> and compares its predictions with experimental results. The model, based on a mathematical development of Muskhelishvili<sup>1,3</sup> embodies the following assumptions: (1) The material outside the plastic zone is elastic, (2) The material within the zone is rigid-perfectly plastic, (3) A Tresca yield criterion is obeyed, (4) Yielding is confined to a narrow wedge-shaped zone.\* Dugdale demonstrated that the plastic-zone size predicted in this way is consistent with the behavior of mild steel. Goodier and Field<sup>11</sup> used the model to calculate crack-tip displacements. Results of further work described in this paper show that silicon steel -- even in the form of reasonably thick plates -- can exhibit a zone similar to that prescribed by the DM (Dugdale-Muskhelishvili) model. Measurements of plastic-zone size and the crack-tip displacement both on-load and after unloading

\*This may be a consequence of the Tresca criterion.

are shown to be in accord with theory. The results also provide insight into the mechanism and conditions favoring the DM zone. The stress gradient in front of the plastic zone is calculated and methods of treating work-hardening and unloading are explored. Finally, implications of the DM model with respect to fracture, particularly crack extension and fracture toughness, are discussed.

PROPERTIES OF THE DM MODEL

Uniform Internal Tension

The DM model is illustrated in Figure 1a. It consists of a slit with an initial length  $2c$  representing a crack in a semi-infinite plate of thickness  $t$ . Under the action of the nominal stress  $T$ , the slit extends to a length  $2a$  and opens, but is partially constrained from extending and opening by a uniformly distributed internal tension of intensity  $S$  acting only on parts of the slit, from  $x = \pm c$  to  $x = \pm a$ , and  $\rho \equiv (a - c)$ . \*\*

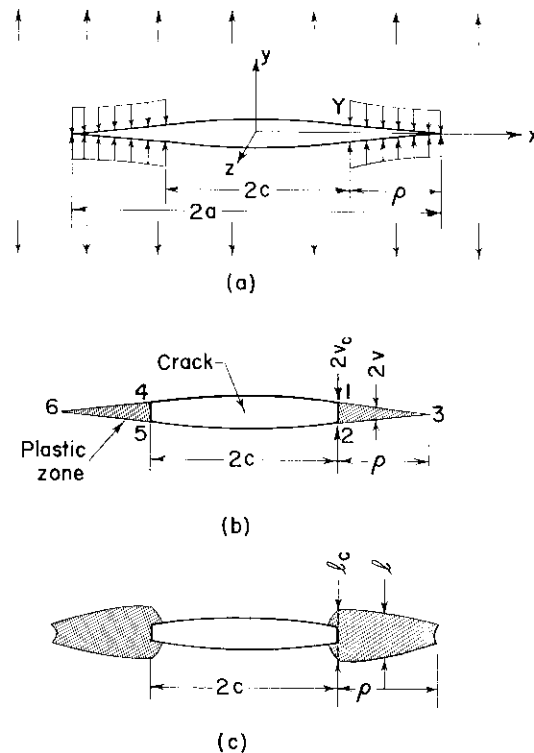


FIG. 1. MODEL OF DUGDALE-MUSKHELISHVILI CRACK. (a) & (b) THE DM MODEL, (c) THE ACTUAL CRACK.

\*\* $S$  is expressed as force per unit length corresponding to unit plate thickness. It is analogous to engineering stress, while  $Y$  is true stress.

Dugdale's basic argument is that if  $S$  is equated with  $Y$  (the yield strength of the material), the internal tension closely simulates the local support derived from similarly shaped wedges of yielded material, which are quite like zones observed experimentally (Fig. 1c). According to the Dugdale hypothesis, Region 1245 (Fig. 1b) represents the partially relaxed crack, and Regions 123 and 456 represent the attending plastic zones. Consistent with this idea, the plastic zones extend as long as the stress at points 3 and 6 (the elastic-plastic boundary) exceeds  $Y$ . By imposing this condition on the stress-field solution (see Appendix, Section 1), Dugdale was able to formulate the plastic-zone size in equilibrium with the applied stress:

$$\frac{\rho}{a} = 2 \sin^2 \frac{\beta}{2} \quad , \quad (1)$$

or

$$\frac{\rho}{c} = \sec \beta - 1 \quad , \quad (2)$$

where  $\beta = \pi T / 2Y$ . The same relations have been derived for the case of a crack in pure shear<sup>11</sup> and torsion.<sup>7</sup>

Although Dugdale derived the stress-field solution (Equation A-1), he did not publish the result or evaluate it numerically. We programmed this equation for a computer and found that the stress gradient for a wide range of applied stress levels is described by the equation (See Appendix, Section 2),

$$\sigma \left( \begin{array}{l} y = 0 \\ x > a \end{array} \right) = T + \frac{T}{\beta} \arctan \left( \frac{\sin 2\beta}{e^{2\alpha} - \cos 2\beta} \right) \quad , \quad (3)$$

where  $\sigma$  is the stress in the  $y$  direction,  $\beta = \pi T / 2Y$ , and  $\alpha = \text{arc cosh } x/a$ . Specific gradients are illustrated in Fig. 2. The DM plastic zone extends farther than the zone derived from the Irwin<sup>2</sup> and Wells<sup>3</sup> assumptions, and about twice as far as the value given by the Inglis elastic solution (the  $x-c/c$  value corresponding to  $Y$ ). It is one-fourth the size of a completely relaxed circular plastic zone<sup>15</sup>. The DM elastic stress field is perturbed (relative to the elastic solutions) a distance  $2\rho$  in front of the crack. Beyond a distance  $2\rho$ , the DM and Inglis solutions converge. The DM model gives the steepest stress gradient near the plastic zone, approaching infinity as  $x \rightarrow a$ . It would appear that material just ahead of a moving crack is subjected to stress rates approaching shock loading.

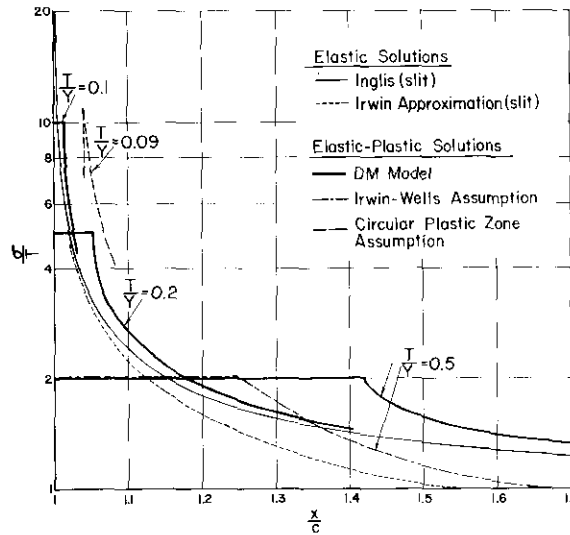


FIG. 2. COMPARISON OF DM STRESS GRADIENTS WITH OTHER SOLUTIONS.

The on-load displacement of a point on the slit wall (see Fig. 1b) has been worked out by Goodier and Field<sup>14</sup> for the DM model,

$$v = \frac{aY}{\pi E} \left( \cos \theta \ln \frac{\sin^2 (\beta - \theta)}{\sin^2 (\beta + \theta)} + \cos \beta \ln \frac{(\sin \beta + \sin \theta)^2}{(\sin \beta - \sin \theta)^2} \right) \quad , \quad (4)$$

where  $v$  is the displacement in the  $y$  direction,  $E$  is Young's modulus,  $\theta = \text{arc cos } x/a$ , and Poisson's ratio is taken as  $1/3$ . Fig. 3 shows

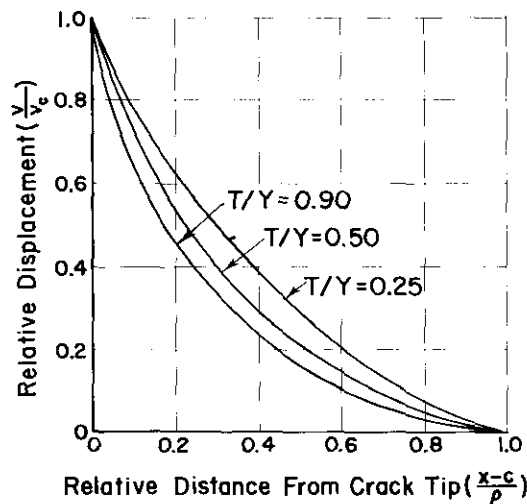


FIG. 3. NORMALIZED DISPLACEMENT-DISTANCE CURVES FOR THE DM MODEL.



that normalized displacement-distance curves for three widely separated values of  $T/Y$  are similar. Goodier and Field<sup>14</sup> also derived an expression for the displacement at the crack tip (Fig. 1b),

$$v_c = \frac{4 Y c}{\pi E} \ln \sec \beta \quad , \quad (5)$$

where  $v_c \equiv v_{(x-c)}$ . Equation (5), presented graphically in Fig. 4, is almost identical to the analogous expression derived by Bilby *et al.*,<sup>11</sup>

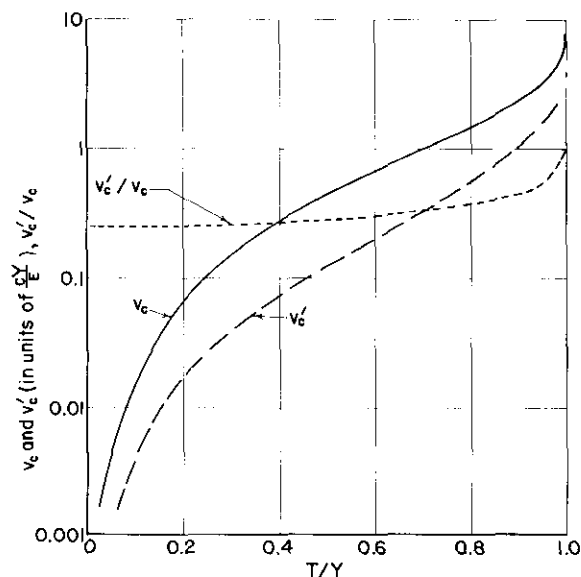


FIG. 4. INFLUENCE OF STRESS LEVEL ON  $v_c$  AND  $v'_c$  THE ON-LOAD AND OFF-LOAD CRACK-TIP DISPLACEMENT AND THE RATIO  $v'_c/v_c$  :

for the case of shear. At low stresses ( $\frac{T}{Y} \lesssim 0.6$ ), Equation (5) reduces to

$$v_c = \frac{\pi c T^2}{2 E Y} \quad . \quad (6)$$

In principle, the operation of the model can also be reversed to simulate unloading. When the load is removed, the opened slit tends to contract and close in response to the internal restoring stress field. But this is now opposed by the enlarged yielded region resisting with a pressure,  $-Y$ , acting on the crack walls from  $c < x < a$ . Under these conditions, the slit contracts as long as the stress at  $x = \pm a$  exceeds  $|Y|$ .

As a useful approximation valid in the vicinity of the crack tip, the restoring stress field

can be replaced by a uniform applied stress  $-T/R$ , such that  $T/R$  will produce in an unconstrained slit (i.e.,  $S = 0$ ) of length  $2a$  the on-load value of  $v/c$  given by Equation (5). As shown in Appendix, Section 3,

$$\frac{T}{R} = \frac{2}{\pi} \cot \beta \ln \sec \beta \quad . \quad (7)$$

The effect of superpositioning  $T/R$  on  $T$  is equivalent to a tension  $(T - T/R)$  acting on a virgin slit,  $2c$ , and this then describes the off-load state in the vicinity of the crack tip:

$$\frac{v'_c}{v_c} = \frac{\ln \sec \beta'}{\ln \sec \beta} \quad , \quad (8)$$

where  $v'_c$  is the off-load crack-tip displacement, and  $\beta' = \pi (T - T/R) / 2Y$ . Values of  $v'_c/v_c$  and the ratio  $v'_c/v_c$  calculated in this way are

reproduced in Fig. 4. The results indicate that  $v'_c/v_c$  approaches 0.25 at low stress and 1 at high stress but is relatively invariant (e.g., 0.25-0.40) in the range  $T/Y = 0-0.85$ .

#### Nonuniform Internal Tension

The calculations outlined so far are valid for a uniform internal tension  $S$  (see Fig. 5a). This is not an unreasonable model for metals provided  $v/c$  is small and the rate of strain hardening is not an important factor. Otherwise, corrections must be applied for (1) the reduction in sheet thickness consistent with plastic deformation at constant volume\* and (2) strain hardening. For example, if deformation is confined to shear on a single  $45^\circ$  slip plane, displacements in the  $y$  direction must be accompanied by a reduction in the load-bearing cross section of the sheet given by  $2v$ . Consequently, if  $Y'$ ,

\*In considering displacements and strains, the following simplifying assumptions consistent with constant volume deformation and the DM model are made:

$$\epsilon = \epsilon_y = \epsilon_z, \epsilon_x = 0;$$

$$v = v_y = v_z, v_x = 0;$$

$$v_y = \int_0^\infty \epsilon_y(y) dy = \int_0^\infty \epsilon_z(y) dy.$$

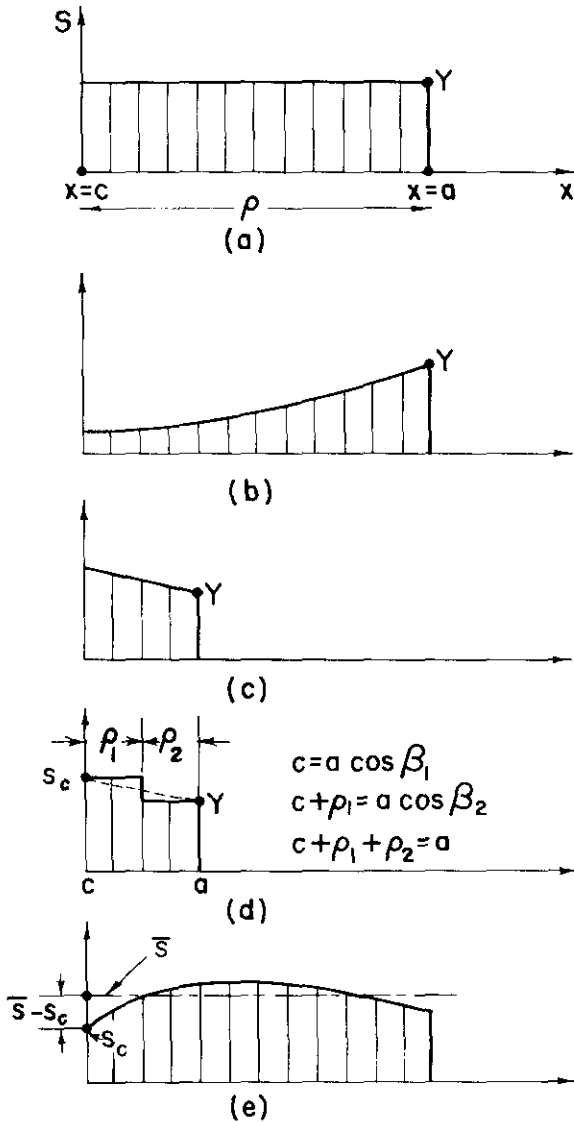


FIG. 5. EXAMPLES OF DIFFERENT DISTRIBUTIONS OF THE INTERNAL TENSION, S.

defined as the true flow stress, is constant (e.g.,  $Y' = Y$ ), the internal tension S, opposing the opening of the crack, must diminish from a maximum value Y at  $x = a$ ,

$$S(x) = Y \left[ 1 - \frac{2v(x)}{t} \right]. \quad (9)$$

This is shown schematically in Figure 5b. If the material also strain hardens, then: (1)  $Y' = Y'(\epsilon)$  where  $\epsilon$  is the strain and (2) the displacement is distributed over a finite volume—a spectrum of strains is now encountered. The reduction in the load-bearing cross section is

$(1 - \epsilon)$ , and the maximum reduction (at  $y = 0$ ) corresponds to the maximum strain  $\epsilon^*$ ,

$$S(x) = Y'(\epsilon^*) [1 - \epsilon^*]. \quad (10)$$

Several points, therefore, emerge about the variable-internal-stress case:

(i) To establish  $S(x)$ , the distribution of strain,  $\epsilon(y)$ , must be known. The model can only provide displacements; strains must be inferred from other considerations or measured experimentally. For example, the displacement can be expressed in terms of  $l$  the width of the plastic zone, and  $\bar{\epsilon}$  the average strain:

$$2v = l \cdot \bar{\epsilon}. \quad (11)$$

Experiments to be described indicate  $l \sim t$ . Since  $\bar{\epsilon} \sim \epsilon^*/2$ ,

$$v \sim \frac{t \epsilon^*}{4}, \quad (12)$$

to a first approximation, and since  $v$  and  $x$  are related by an equation analogous to Equation (4),

$$S(x) \sim Y'(v) \left[ 1 - \frac{4v}{t} \right]. \quad (13)$$

If the internal stress distribution can be defined, then, as shown in Appendix, Section 4, the corresponding  $\rho$ ,  $\sigma(x)$ , and  $v(x)$  can be calculated.

(ii) Equations (10) and (13) show that the form of  $S(x)$  is similar to a load elongation curve. Since strain hardening and the variation of  $v$  with  $x$  are essentially parabolic, the initial part of  $S(x)$  is linear (see Fig. 5c). A two-step function (see Fig. 5d) is thus a convenient approximation of small yielded zones. This approximation, together with Equation (13), was used to estimate the influence of work hardening on plastic-zone size for silicon steel (see Appendix, Section 5). The results, presented graphically in Fig. 6, indicate that the influence of strain hardening becomes significant for long cracks and high stress levels.

Another simple approximation, which takes into account the effect of work hardening on  $v'/c$ , is to modify the definition of  $\beta'$  in Equation (8) by replacing  $Y$  with  $S/c \equiv S/(x=c)$ , the flow stress corresponding to the maximum strain at the crack tip. This simple approximation neglects the Bauschinger effect.

The form of  $S(x)$  at high stress levels is illustrated in Fig. 5e. In this case, the instan-

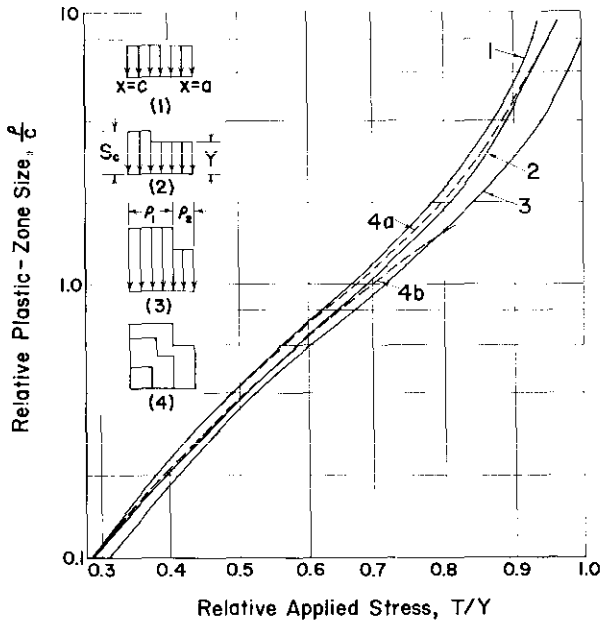


FIG. 6. EFFECT OF WORK HARDENING ON THE RELATION BETWEEN APPLIED STRESS AND PLASTIC-ZONE SIZE.

- (1) Uniformly Distributed Internal Tension
- (2) Two-Step Distribution ( $S_c/Y = 1.20$ ,  
 $\rho_1 = 0.5 \rho_2$ )
- (3) Two-Step Distribution ( $S_c/Y = 1.33$ ,  
 $\rho_1 = 2.0 \rho_2$ )
- (4) Varying Distribution Simulating Work Hardening: (a)  $c/t = 6.25$ , (b)  $c/t = 25.0$

taneous average  $\bar{S}$  can serve as a useful approximation of the distribution, e.g., Equation (2),

$$\frac{\rho}{c} = \sec \frac{\pi T}{2\bar{S}} - 1 \quad (2A)$$

where

$$\bar{S} \approx \frac{U + F}{2} \quad (14)$$

and U and F are the ultimate tensile strength and fracture strength, both expressed in terms of engineering stress.

(iii) The shape of the plastic zone consistent with the mechanism of deformation will not necessarily correspond with the shape prescribed by the DM model. This could be taken into account by modifying the geometry of the DM model — replacing the slit by some other shape — but the refinement may not warrant the added complications.

The main problem, to be resolved by experiments, is the extent to which approximations inherent in the DM model impair the accuracy of its predictions. Dugdale<sup>12</sup> has already shown that the model gives a reasonable picture of the plastic-zone size in mild steel. The experiments described in the next two sections show that measurements of plastic-zone size and crack-tip displacements for silicon steel are also in accord with the theory.

#### EXPERIMENTAL PROCEDURE

Studies of locally yielded zones were carried out on large notched test coupons fabricated from 3% silicon steel (Si 3.31, C 0.04). The coupons (over-all length 8 inches, with a 4 x 2.5-inch gage section, and with centrally located edge slots 0.25 inch deep and 0.006 in. wide), derived from 1/4-inch-thick plate previously warm rolled 40% and stress relieved, were machined to thicknesses from 0.232 to 0.017 in. After machining, the coupons were recrystallized at 875 C and slowly cooled. The test specimens were loaded to various stress levels, held at maximum load for about five seconds, unloaded, and later aged for 20 minutes at 150 C to decorate the dislocations. The stress-strain characteristics of this material in the annealed condition are shown in Fig. A1. The shape of the stress-strain curve is similar to that of a mild structural steel, but the strength level is higher, the lower yield stress  $Y = 62,400$  psi. A complete summary of tests performed is given in Table 1.

Two different techniques were employed to reveal the plastic zone and the strain distribution within the zone. The off-load transverse strain field was photographed on an interference microscope. The interference pattern with iso-strain contours and the corresponding strain profile for Sample S-56 are shown in Figs. 7 and 8. The strain profile was used to calculate

$$v' \quad (v' = \int_0^{\infty} \epsilon_z \, dy).$$

Following this, the surfaces of the test pieces were electro-polished and etched, utilizing the Morris procedure,<sup>16</sup> to reveal the plastic zone, and then were reground to various depths, polished, and re-etched to delineate the zone on various interior sections. This method of etching, based on the preferential attack of individual dislocations, results in a gradual darkening of the surface as the strain

TABLE 1. SUMMARY OF NOTCH TESTS PERFORMED.

Specimen Number	Thickness, inch	T/Y	Zone Type	$\rho$ -Measured, inch	$\rho$ -Calculated <sup>(b)</sup> , inch	$\rho$ -Calculated <sup>(c)</sup> , inch
S-57	0.200	0.52	Hinge <sup>(d)</sup>	$\rho^H$ <sup>(d)</sup> = 0.072	0.12	--
S-60	0.195	0.81	Transition	$\rho^H$ = 0.54	0.58	0.40
S-58	0.232	0.90	45°-Shear	$\rho^{II}$ > 1.40 <sup>(a)</sup> $\rho$ = 0.60	1.35	1.20
S-47	0.165	0.75	Transition			
S-48	0.128	0.90	45°-Shear			
S-53	0.060	0.78	45°-Shear	$\rho$ = 0.38	0.48	0.44
S-55	0.017	0.52	45°-Shear	$\rho$ = 0.10	0.12	0.10
S-56	0.017	0.81	45°-Shear	$\rho$ = 0.39	0.58	0.40

(a) Although, in this sample, yielding was predominantly of the 45°-shear type, traces of plastic deformation of a hinge character were observed to the distance indicated.

(b) Calculated from Equation (1) assuming no work hardening.

(c) Calculated taking work hardening into account (Figure 6 and Appendix, Section 5).

(d) See Figure 11 for definition of  $\rho^H$ .



FIG. 7. INTERFERENCE PATTERN WITH ISO-STRAIN CONTOURS (TOP LEFT CORNER) AND THE CORRESPONDING PLASTIC ZONE REVEALED BY ETCHING, BOTH FOR SAMPLE S-56 ( $t = 0.017$  inch,  $T/Y = 0.81$ ). 20X

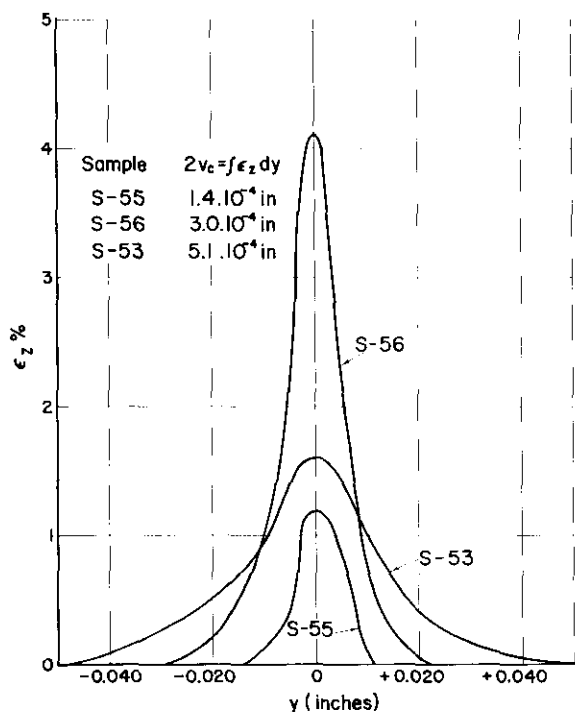


FIG. 8. CRACK-TIP STRAIN PROFILES DETERMINED FROM INTERFEROMETRIC MEASUREMENT.

increases to 1-2%. Beyond 2% strain the etching response diminishes, and above about 5% strain the material studied here was not attacked, probably because decoration was incomplete. Consequently, the technique revealed both the extent of the plastic zone and, to some degree, the distribution of strain within the zone. The change in etching response is illustrated in Fig. 7 which shows a highly strained but unetched region close to the notch tip. A displacement  $v/e$  can be calculated from  $t/e$ , the width of the etched region, and  $\bar{\epsilon}/e$ , an average strain, deduced from the etching response, see Equation (11). Since  $v/e = v + (v - v')$ , the sum of absolute values of displacement incurred when the load is applied plus the reverse displacement produced by unloading, it can be combined with  $v'$  from the interferometric measurement to give  $v$ , the on-load displacement,

$$v = \frac{v_e + v'}{2} \quad (15)$$

### EXPERIMENTAL RESULTS

The interpretation of plastic zones revealed by etching is complicated by the fact that yielding concurrent with loading is superimposed on reverse flow during unloading. Still, a reason-

able picture emerges of the effect of stress and plate thickness on the character of the plastic zone. Three types of plastic zones are observed (see Figs. 7, 9, and 10):

1. Hinge-Type Zone. At low-stress levels the zone extends normal to the plane of the crack, and its form is essentially the same on all interior sections (see Figs. 9a and 9b). The shape of the zone is consistent with the idea that yielding occurs essentially by flow about hypothetical plastic hinges<sup>17</sup> (see Fig. 11). The hinge-type zone is also qualitatively in accord with Jacobs zone-shape calculations for plane strain.<sup>5</sup>
2. 45-Degree Shear-Type Zone. At high-stress levels the zone is projected in front of the crack in the direction parallel to the crack plane. As shown in Figs. 7b, 9e, 9f, 10d, and 10c, this form bears a striking resemblance to the DM model. Etching the interior sections reveals that the mechanism of yielding in this case is shear on slabs inclined ~45 degrees to the tensile axis, similar to necking of unnotched sheet coupons (see Fig. 11). As a consequence of the 45°-shear nature of the yielding, the zone width on the surface is approximately equal to the plate thickness; this is shown in Figs. 10e and 11c.
3. Transition Zone. At intermediate stresses, the zone appears in a state of transition between the hinge type and 45°-shear type (see Figs. 9c, 9d, 10a, and 10b).

Measurements of the zone size (summarized in Table 1) are in accord with previous experience. Consistent with Tetelman,<sup>13</sup>  $\rho^H$  (see Fig. 11) for the hinge-type zone of Sample S-57 is described by

$$\frac{\rho^H}{c} \sim \frac{1}{2} \left( \sec \frac{\pi T}{2Y} - 1 \right) \quad (16)$$

The extent of the 45°-shear-type zone of Sample S-55 is in good agreement with Equation (2). Values for Samples S-56, S-63, S-48, and S-58 are somewhat smaller than predicted. Although better agreement is obtained when work hardening is taken into account (see Table 1), a discrepancy remains. This could be related to departures from the infinite plate solution (likely when the plastic zone covers more than 20-30% of the sample cross-section area) and to the fact that the DM model only approximates the shape of real zones.

The results summarized in Table 2 represent the first attempt to check displacement values predicted by the DM model. As shown, both the

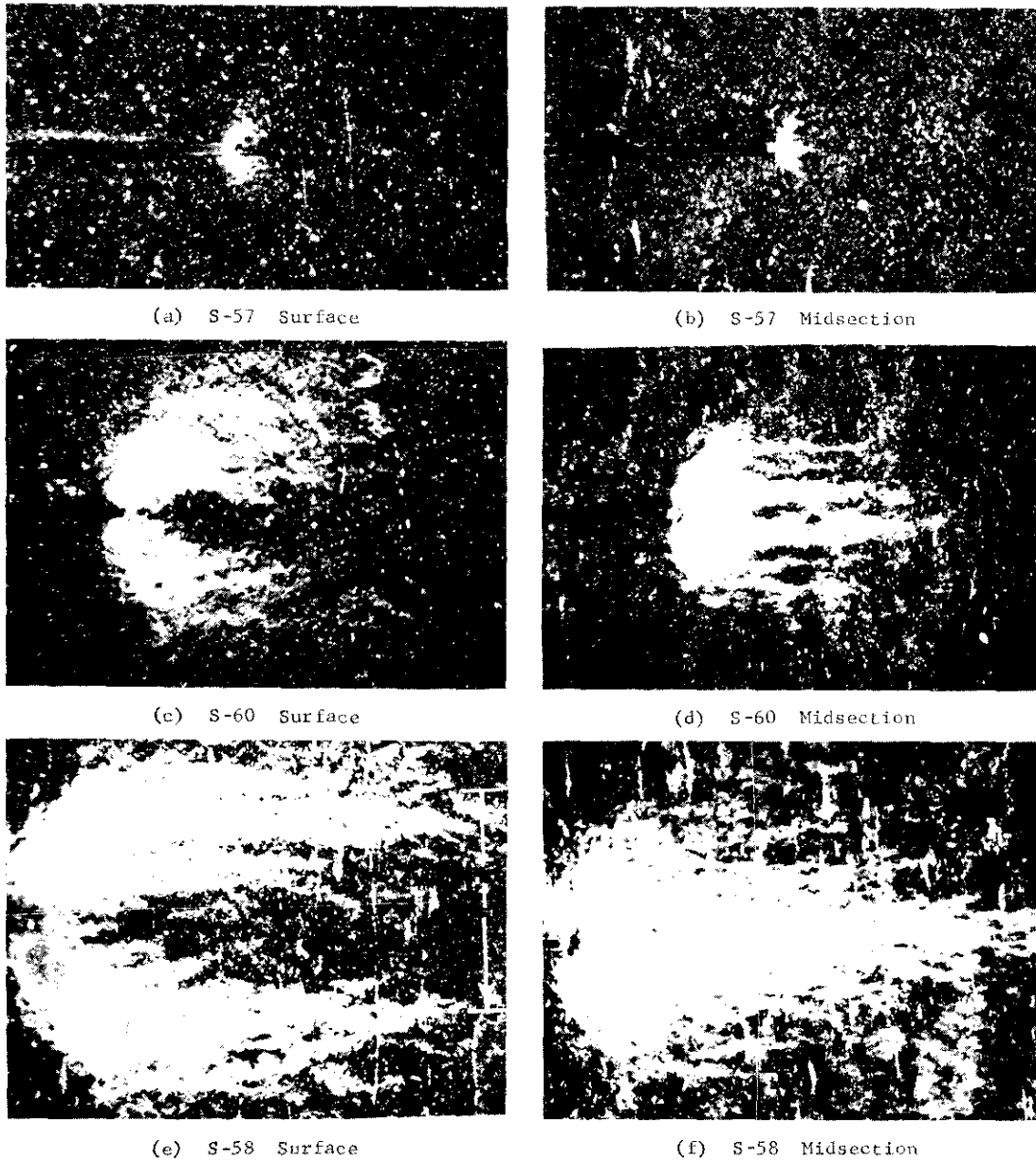


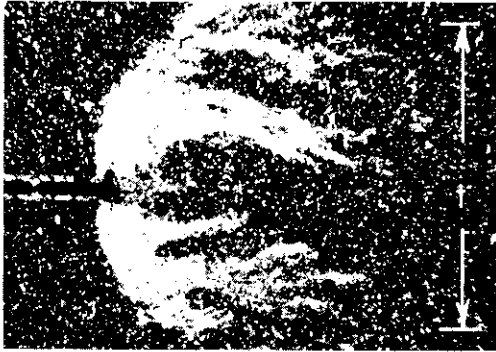
FIG. 9. PLASTIC ZONES REVEALED BY ETCHING THE SURFACE AND MIDSECTION OF NOTCHED COUPONS:

- (a) and (b) Sample S-57 ( $t = 0.200$  inch,  $T/Y = 0.52$ )
  - (c) and (d) Sample S-60 ( $t = 0.195$  inch,  $T/Y = 0.81$ )
  - (e) and (f) Sample S-58 ( $t = 0.232$  inch,  $T/Y = 0.90$ )
- Oblique illumination, 5.5 X

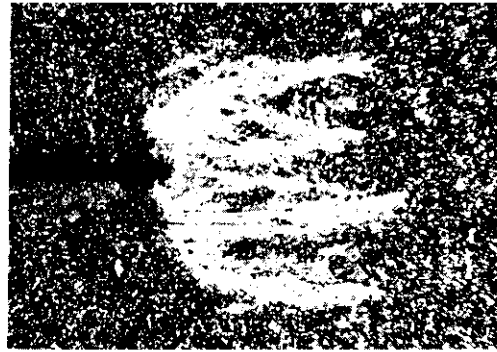
on-load and off-load crack-tip displacement values derived from the etching response and the interferometric measurements are in reasonable accord with the theory. Work-hardening corrections do not improve the agreement in  $v/c$  values for Samples S-53 and S-55; in both cases the maximum strain is small, and the Bauschinger effect could be more important than strain hard-

ening.

On the basis of these results, it appears that the DM model offers a useful description of (a) shape, (b) size, and (c) displacements of a 45°-shear-type plastic zone. Two points bearing on the general applicability of the model should be kept in mind:



(a) S-47 - Surface



(b) S-47 - Midsection



(c) S-48 - Surface

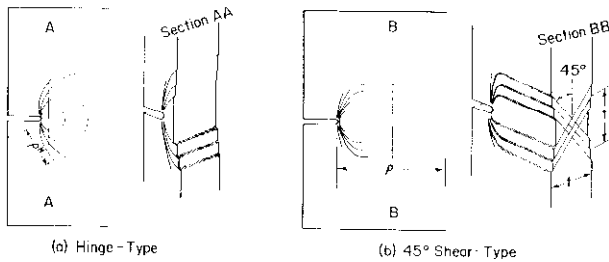


(d) S-48 - Midsection

FIG. 10. PLASTIC ZONES REVEALED BY ETCHING THE SURFACE AND THE MIDSECTION OF NOTCHED COUPONS:

- (a) and (b) Sample S-47 ( $t = 0.165$  inch,  $T/Y = 0.75$ )
- (c) and (d) Sample S-48 ( $t = 0.128$  inch,  $T/Y = 0.90$ )

Oblique illumination 9.5X



(a) Hinge-Type

(b) 45° Shear-Type

FIG. 11. SCHEMATIC DRAWING OF THE TYPE OF DEFORMATION ASSOCIATED WITH (a) THE HINGE-TYPE AND (b) THE 45°-SHEAR-TYPE PLASTIC ZONE.

(i) First, the state of stress must be substantially plane stress. The 45°-shear mode will be constrained until the stress acting on regions a distance  $t/2$  above and below the crack center-line,  $y = 0$  (see Fig. 11), exceeds the yield

stress. Yielding at this distance first becomes possible when

$$\rho^H > \frac{t}{2}, \quad (17)$$

and this condition should approximately mark the beginning of the transition from the hinge-type to the 45°-shear-type zone. The configuration begins to approach a narrow, tapered DM-model zone when

$$\rho \sim 4t, \quad (18)$$

since the zone width is  $\sim t$ . Limiting conditions for the various types of zones, formulated by combining Equations (18) with (2) and (16) with (17), are summarized in Table 3. These conditions are consistent with the experimental observations.

(ii) The 45°-shear zone has, so far, only been observed in steel. In fact, the Stimpson and Eaton<sup>10</sup> theoretical calculations for plane stress

TABLE 2. COMPARISON OF MEASURED CRACK-TIP DISPLACEMENT VALUES WITH PREDICTIONS OF THE DM MODEL.

Sample Number	T/Y	Derived from Measurements (a)					Calculated		
		$l_{ce}$ , inch	$\bar{\epsilon}_{ce}$ , %	$v_{ce}$ , $10^{-4}$ inch	$v_c^r$ , $10^{-4}$ inch	$v_c$ , $10^{-4}$ inch	$v_c^r$ (b), $10^{-4}$ inch	$v_c^r$ (c), $10^{-4}$ inch	$v_c$ (d), $10^{-4}$ inch
S-55	0.52	0.026	3 - 4	4 - 6	0.7	2 - 3	0.8	0.9	2.5
S-56	0.81	0.044	4 - 7	10 - 14	3.4	6 - 9	3.1	3.7	8.1
S-53	0.78	0.063	3 - 4	18 - 24	2.1	6 - 7	2.6	3.1	7.0

- (a) The quantities  $l_{ce}$ ,  $\bar{\epsilon}_{ce}$ , and  $v_{ce}$  are the average width, strain, and displacement, respectively, immediately in front of the slot as revealed by etching.  $v_{ce} \approx 1/2 l_{ce} \bar{\epsilon}_{ce}$ .  $v_c^r$  is derived from the interference pattern as described in the text.  $v_c$  is calculated from  $v_{ce}$  and  $v_c^r$  via Equation (15).
- (b) Calculated from Equations (7) and (8) using:  $Y = 62,400$  psi,  $E = 30,000,000$  psi, and  $C = 0.250$  inch.
- (c) These values of the off-load displacement were calculated taking work hardening into account as described in paragraph (ii) on page 12 and page 13.
- (d) Calculated from Equation (5).

TABLE 3. LIMITING CONDITIONS FOR ZONE OCCURRENCE.

Condition	Dominant Zone
$\frac{t}{c} < (\sec \frac{\pi T}{2Y} - 1)$	Hinge type
$(\sec \frac{\pi T}{2Y} - 1) < \frac{t}{c} < \frac{1}{\lambda} (\sec \frac{\pi T}{2Y} - 1)$	Transition
$\frac{t}{c} > \frac{1}{\lambda} (\sec \frac{\pi T}{2Y} - 1)$	45°-shear type

do not predict a 45°-shear zone, but a shape with much more "hinge" character. Even when the bulk of the deformation is of the 45°-shear type, the silicon steel exhibits traces of deformation at distances  $y > t/2$  (see Fig. 7 and  $\rho^H$  for Samples S-60 and S-58 in Table 1), in keeping with the calculations. The discrepancy between the Stimpson and Eaton calculations and the behavior of steel may be related to the choice of yield criterion (von Mises, as opposed to Tresca, in the case of the DM model), or to the yield point effect.<sup>1,11</sup> Until this point is resolved, the safest assumption is that the 45-degree-shear-type zone is one of several modes of relaxation possible under plane stress.

IMPLICATIONS FOR FRACTURE

Since it is both quantitatively meaningful and simple to handle, the DM model is especially useful in dealing with fracture. It can approximate the stress-strain-rate environment in front of a propagating crack.<sup>1,5</sup> It may have application to fatigue, since it can deal with loading

and unloading. Finally, the DM model can be used to treat crack extension. In this case, the predictions of the model complement accepted theory and experiment and for this reason are outlined below.

Equation (6), for the crack-tip displacement when  $T/Y < 0.6$ , can be written

$$T = \left( \frac{2 v_c Y E}{\pi C} \right)^{1/2} \quad (19)$$

and, in this form, compared with Irwin's basic condition for crack extension,

$$T^* = \frac{K_c}{(\pi C)^{1/2}} \quad (20)$$

In this case,  $T^*$  is the critical stress for crack extension, and  $K/c$  (the fracture toughness) is an empirical measure of the material's resistance to cracking.<sup>2,9</sup> The fact that Equations (19) and (20) have the same form implies that  $K/C$  is related to  $v/c$  and can be calculated directly,

$$K_c = (2 v_c^* Y E)^{1/2} \quad (21)$$

where  $v^*/c$  represents the crack-tip displacement at crack extension. The connection between  $v^*/c$  and  $K/c$  was first recognized by Wells,<sup>2,1</sup> and an expression similar to Equation (21) has been derived by Bilby et al.<sup>1,1</sup>

Since  $K/c$  and  $Y$  are material constants, the



quantity  $v^*/c$  must also be constant. The constancy of  $v^*/c$  can be related to invariance on the part of  $\epsilon^*/c$ , a critical maximum crack-tip strain, via Equations (11) and (12). Two mechanisms of crack extension can be related to a specific strain level:

1. Ductile Fracture. Ductile fracture by the process of voids coalescing<sup>22</sup> might be expected to occur just in front of the crack tip when the maximum strain at this point reaches a level comparable to the reduction in area of an unnotched coupon,

$$\epsilon_c^* = RA \quad (22)$$

The crack then grows a small increment, and the maximum strain must increase further

$$\left( \frac{\partial \epsilon_c^*}{\partial c} \right)_{T,Y} > 0, \quad \text{see Equations (5) and (12).}$$

Since the strain at the crack tip is already beyond the capabilities of the material, an instability is inevitable. Locally, the origin of such failures is ductile fracture, but they are frequently classified as brittle when the failure stress is below the stress level for general yielding.

As shown in Table 4,  $K/c$  values, calculated directly from Equations (12), (21), and (22), for 4330 steel and 2219-T87 aluminum are reasonably consistent with experiment,<sup>23</sup> considering the approximations made. If the relation between  $v^*/c$  and  $\epsilon^*/c$  were known more precisely,

even better agreement might be obtained.  
 2. Plastic Instability. Another possibility is that the plastic zone become unstable first, and that ductile fracture (and crack extension) follows in the wake of the instability. This idea, which was recently proposed by Krafft,<sup>24</sup> can be formulated using the DM model. As shown in the Appendix, Section 6, the instability condition is approximately

$$\left( \frac{\bar{S} - S_c}{\bar{S}} \right) > \quad (23)$$

$$\left[ \sec \frac{\pi T}{2\bar{S}} - 1 \right] \left[ \left( \frac{\pi T}{2\bar{S}} \right) \left( \sec \frac{\pi T}{2\bar{S}} \right) \left( \tan \frac{\pi T}{2\bar{S}} \right) \right]^{-1}.$$

Figure 12, a plot of the criterion of Equation (23) shows that considerable unloading is tolerated at low stress levels (e.g.,  $T/\bar{S} < 0.7$ ), but the plastic zone becomes unstable as a result of a small decrease in  $S/c$  when the stress is high (e.g.,  $T/\bar{S} > 0.7$ ). Consequently, plastic instability is the more likely mechanism of crack extension at high stress if the material is reasonably ductile.

According to this picture,  $v^*/c$  and  $\epsilon^*/c$  associated with plastic instability (and failure) decrease as the stress is raised. Since Equation (21) is not valid at high stresses, a simple

TABLE 4. COMPARISON OF MEASURED AND PREDICTED VALUES OF THE FRACTURE TOUGHNESS  $K/c$  AND GROSS FAILURE STRESS  $T^*$ .

Material	Critical Crack Length, Inch	$K_c$ , ksi/inch		$T^*$ , psi	
		Measured <sup>(23)</sup>	Calculated <sup>(c)</sup>	Measured <sup>(23)</sup>	Calculated <sup>(d)</sup>
A. Low Stress Levels, $T/\bar{S} < 0.7$ <sup>(e)</sup>					
4330 <sup>(a)</sup>	2-10	300	420		
2219-T87 <sup>(b)</sup>	5-15	110	99		
B. High Stress Levels, $T/\bar{S} > 0.7$ <sup>(e)</sup>					
4330 <sup>(a)</sup>	0.5			90,000	200,000
2219-T87 <sup>(b)</sup>	0.8			57,000	58,000
"	1.5			59,000	53,000

(a) 4330 steel data<sup>(23)</sup>  
 $t = 0.140$  inch,  $E = 30,000,000$  psi,  $Y = 189,000$  psi,  $U = 223,000$  psi,  
 $\bar{S} = 206,000$  psi,  $F = 178,000$  psi,  $RA = 47\%$ ,  $\epsilon_u = 67\%$ .

(b) 2219-T87 aluminum data<sup>(23)</sup>  
 $t = 0.100$ ,  $E = 11,000,000$  psi,  $Y = 59,000$  psi,  $U = 69,000$  psi,  
 $\bar{S} = 64,000$  psi,  $F = 56,000$  psi,  $RA = 30\%$ ,  $\epsilon_u = 72\%$ .

(c) Equations (12), (21), and (22).

(d) Equations (12), (23), and (2b).

(e)  $\bar{S} = \frac{Y+U}{2}$ .

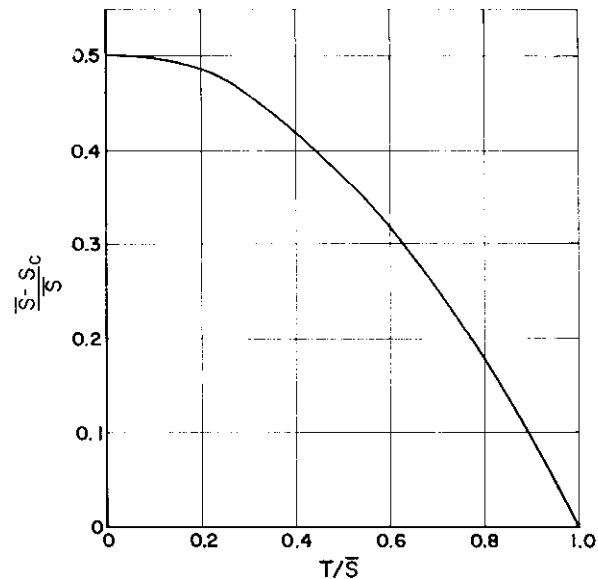


FIG. 12. CRITERION FOR PLASTIC INSTABILITY OF A DM ZONE.

relation among  $K/c$ ,  $T^*$ , and  $c$  cannot be derived. However, the value of  $\epsilon^*/c$  at instability can be estimated (see Appendix, Section 6),

$$\epsilon_c^* \approx \epsilon_u + \sqrt{H \left( \frac{\bar{\sigma} - \sigma_c}{\bar{\sigma}} \right)}, \quad (24)$$

where

$$H = (\epsilon_f - \epsilon_u)^2 \left( \frac{U-F}{U} \right)^{-1}, \quad \text{and } U \text{ and } F$$

are the ultimate tensile stress and fracture stress (engineering stress), and  $\epsilon/u$  and  $\epsilon/f$  are the corresponding strains (expressed as reduction in area). Equations (24), (12), and (23) together fix the value of  $T$  at instability. As shown in Table 4, failure stress values calculated in this way are in good accord with actual measurements and consistent with the apparent decrease of  $K/c$  observed at high stress levels, i.e.,  $T/Y > 0.8$ .<sup>2,3</sup>

## CONCLUSIONS

1. For edge-slotted silicon steel, local yielding is predominantly of the plane strain plastic-hinge type until the extent of the yielded zone is about equal to the sheet thickness. Further deformation, under plane stress conditions, proceeds by a 45-degree-shear mode.

2. The general shape of the 45-degree-shear zone can approach that of the DM (Dugdale-Muskhelishvili) crack model. Predictions of this model are in agreement with measured zone size and displacement values for silicon steel.

3. The DM model offers a relatively simple expression of the stress gradient and can be used to estimate effects of work hardening and unloading. Calculations and experiments indicate that the off-load crack-tip displacement approaches 25% of the on-load value at low stress.

4. The DM model can be used to formulate the conditions for crack extension. Failure stress values and the fracture toughness,  $K/c$ , calculated in this way from first principles, are in accord with experiment.

## ACKNOWLEDGMENTS

The authors are indebted to the American Gas Association and the Ship Structure Committee for their support of the theoretical and experimental aspects of this paper, respectively. Mr. Paul Mincer, of Battelle, provided technical assistance.

## REFERENCES

1. C. E. Inglis, Trans, Inst. Naval Arch., London, 55, 219 (1913).
2. G. R. Irwin, J. Appl. Mech., 24, 361 (1957).
3. A. A. Wells, Brit. Weld. J., 10, 855 (1963).
4. D. N. deG. Allen and R. V. Southwell, Phil. Trans. Roy. Soc., A242, 379 (1950).
5. J. A. Jacobs, Phil. Mag., 41, 349 (1950).
6. L. D. Stimpson and D. M. Eaton, Technical Report ARL24, California Inst. of Tech., 1961.
7. J. A. H. Hult and F. A. McClintock, 9th Int. Cong. Appl. Mech., 8, 51 (1957).
8. F. A. McClintock, Materials Research & Standards, 1, 277 (1961).
9. F. A. McClintock, Drucker & Gilman, eds., Fracture of Solids, Interscience Publishers, New York (1963), p. 65.
10. J. F. Knott and A. H. Cottrell, J. Iron Steel Inst., 201, 249 (1963).
11. B. A. Bilby, A. H. Cottrell, and K. H. Swinden, Proc. Roy. Soc., A272, 304 (1963).
12. D. S. Dugdale, J. Mech. Phys. Solids, 8, 100 (1960).
13. N. I. Muskhelishvili, Some Basic Problems of the Mathematical Theory of Elasticity, Noordhoff, Groningen (1953), p 340.
14. J. N. Goodier and F. A. Field, Drucker and Gilman, eds., Fracture of Solids, Interscience Publishers, New York (1963), p 103.
15. G. T. Hahn, A. Gilbert, and C. N. Reid, J. Iron Steel Inst., 202, (1964).
16. C. E. Morris, Metal Progress, 56, 696 (1949).
17. A. P. Green and B. B. Hundy, J. Mech. Phys. Solids, 4, 128 (1956).
18. A. S. Tetelman, Acta Met. (in press).

19. J. L. Swedlow, California Institute of Technology; private communication, 1964.
20. G. R. Irwin, Metals Engineering Quarterly, 3, 24 (1963).
21. A. A. Wells, Proceedings of Crack Propagation Symposium, 1961, sponsored by Roy. Aer. Soc., published by College of Aeronautics, Cranfield, England (1962), 1, 210.
22. H. C. Rogers, Trans. AIME, 218, 498 (1960).
23. ASTM Committee on Fracture Testing of High Strength Materials, Materials Research & Standards, 4, 107 (1964).
24. J. M. Krafft, Applied Materials Research 3, 88 (1964).

APPENDIX

1. Previous Work

Using Muskhelishvili's<sup>(13)</sup> method, the normal stress,  $\sigma$ , in front of a slit subjected to the stress system shown in Figure 1 is found to be

$$\sigma_{y=0, x>a} = \left(T - \frac{2\beta Y}{\pi}\right) \coth \alpha + T \left\{ 1 - \frac{1}{\beta} \arctan \frac{\sin 2\beta}{\cos 2\beta - e^{2\alpha}} - \frac{Q e^{\alpha}}{4\beta} \right\}, \quad (A-1)$$

where  $T$  = applied stress,  $Y$  = yield stress,  $\cos \beta = c/a$ ,  $\cosh \alpha = x/a$ ,

$$Q = \frac{\delta'_A \cosh \alpha}{(\sinh \alpha)^3} \left\{ 3 [\sinh \alpha]^2 + \cosh \alpha \sinh \alpha - 1 \right\} + \delta'_A (\coth \alpha)^2 \left[ 1 - \frac{\delta'_A e^{\alpha} (e^{2\alpha} - \cos 2\beta)}{\sin 2\beta} \right] - \frac{\delta'_B \cos \beta}{(\sinh \alpha)^3} \left\{ 3 [\sinh \alpha]^2 + \cosh \alpha \sinh \alpha - [\cosh \alpha]^2 \right\} - \frac{\delta'_B e^{\alpha} \cos \beta}{(\sinh \alpha)^2} \left[ 1 + \frac{\delta'_B (1 - e^{2\alpha} - 2 [\sin \beta]^2)}{2 \sin \beta} \right],$$

$$\delta'_A = \frac{4 \sin 2\beta e^{\alpha}}{(e^{2\alpha} - \cos 2\beta)^2 + (\sin 2\beta)^2}, \quad \text{and} \quad \delta'_B = \frac{4 \sin \beta (1 + e^{2\alpha})}{(1 + e^{2\alpha})^2 - (2e^{\alpha} \cos \beta)^2}.$$

The other terms of Equation (A-1) are defined in Figure 1. To avoid the infinity at  $\alpha = 0$  ( $x = a$ ), the coefficient of  $\coth \alpha$  must vanish:

$$\beta = \frac{\pi}{2} \frac{T}{Y} = \arccos (c/a) \quad . \quad (A-2)$$

2. Stress Analysis for Uniformly Loaded Slit

Equation (A-1) was programmed for a digital computer and  $\sigma$  and  $Q$  determined for 792 combinations of  $\alpha$  and  $\beta$ . It was found that  $Q$  was

negligibly small, except for values of  $\alpha$  so small as to introduce rounding off errors in the computer ( $\frac{x}{a} < 1.0002$  and  $\frac{T}{Y} < 0.006$ ). It can also be shown by series approximations that  $Q$  approaches 0 as  $\alpha$  approaches 0. We have concluded that  $Q$  can be ignored, and that

$$\frac{\sigma}{T} = 1 + \frac{1}{\beta} \arctan \left\{ \frac{\sin 2\beta}{e^{2\alpha} - \cos 2\beta} \right\} . \quad (A-3)$$

### 3. Displacement

The displacement at any point on a slit under a uniform tension when the slit is not restrained by an internal stress is

$$v = \frac{(k + 1) a T \sin \theta}{4\mu} , \quad (A-4)$$

$k$  is the function of Poisson's ratio,  $\nu$ , where  $k = (3 - \nu)/(1 + \nu)$  for plane stress. The displacement at a distance,  $c$ , from the center of such a slit is

$$v_c = \frac{(k + 1) c T \tan \beta}{4\mu} \quad (A-5)$$

since  $c/a = \cos \beta$ , and  $\theta = \beta$ .

The displacement equations for the relaxed slit of the DM model have been calculated by Goodier and Field,<sup>(14)</sup> and are found in the body of the paper. In particular, the critical displacement for an internally stressed slit (see Figure 1a) is

$$v_c = \frac{(k + 1) cY}{2\mu\pi} \ln \sec \beta . \quad (A-6)$$

To determine the stress,  $T_r$ , producing the same displacement in a slit of the same length in the absence of an internal stress, (A-6) is substituted into (A-5)

$$\frac{T_R}{Y} = \frac{2}{\pi} \cot \beta \ln \sec \beta . \quad (A-7)$$

4. Stress and Plastic-Zone Size for Arbitrarily Loaded Slit

Since all terms in the Muskhelishvili formulation which involve derivatives of  $\delta_A$  and  $\delta_B$  do not appear in Equation (A-3), expressions for a slit subjected to any arbitrary combination of internal and external loads can be derived easily. For example, the stress distribution in front of the slit of Figure 5d can be found by the summation of three solutions

$$(\sigma = \sigma_1 + \sigma_2 + \sigma_3):$$

(1) External tensile stress,  $\sigma_1 = T \coth \alpha$  (A-8)

(2) Uniform internal pressure,  $-S_c$ , applied to the regions

$$|a| > |x| > |c| : \sigma_2 = \frac{-S_c}{\pi} \left\{ 2\beta_1 [\coth \alpha - 1] + \delta_A(\beta_1) \right\} \quad (A-9)$$

(3) Uniform internal pressure ( $S_c - Y$ ) applied to the regions

$$|a| > |x| > (|c| + |p_1|) : \sigma_3 = \frac{S_c - Y}{\pi} \left\{ 2\beta_2 [\coth \alpha - 1] + \delta_A(\beta_2) \right\} \quad (A-10)$$

where 
$$\delta_A = -2 \arctan \left( \frac{\sin 2\beta}{e^{2\alpha} - \cos 2\beta} \right) .$$

Setting the coefficient of  $\coth \alpha$  equal to 0, results in the restriction,

$$\frac{\pi T}{2} = (\beta_1 - \beta_2) S_c + \beta_2 Y \quad , \quad (A-11)$$

and the solution

$$\frac{\sigma}{T} = 1 + \frac{\delta_A(\beta_2)}{\pi T} (S_c - Y) - \frac{\delta_A(\beta_1) S_c}{\pi T} \quad . \quad (A-12)$$

Keeping the same boundary conditions ( $S = S_c$  at  $\beta = \beta_1$  and  $S = Y$  at  $\beta = 0$ ), but letting  $S(\beta)$  now be an arbitrary function of  $\beta$ , Equations (A-8) and (A-9) can be added to

$$\sigma_3 = \frac{1}{\pi} \int_{S_c}^Y \left\{ 2\beta [\coth \alpha - 1] + \delta_A(\beta) \right\} dS(\beta) \quad , \quad (A-10a)$$

to give  $\sigma$  and the restriction,

$$\frac{\pi T}{2} = \beta_1 S_c + \int_{S_c}^Y \beta dS(\beta) \quad . \quad (A-11a)$$

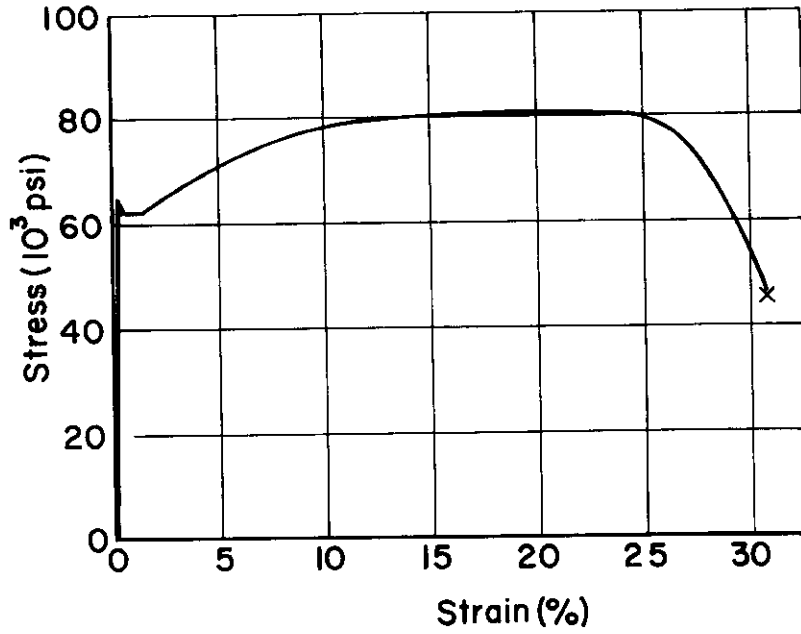
The displacements for an arbitrarily loaded slit can be obtained by replacing  $Y$  in Equation (4) with

$$Y_c + \frac{1}{\beta_1} \int_{S_c}^Y \beta dS(\beta) \quad .$$

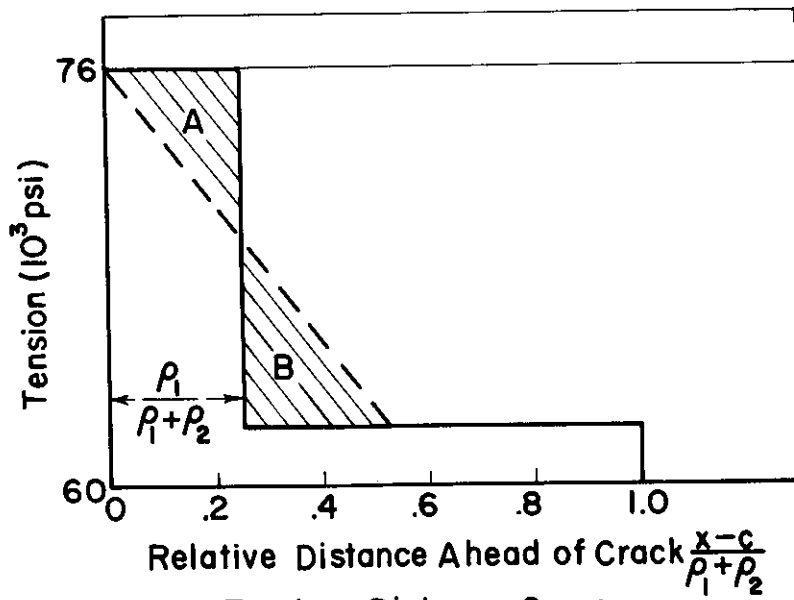
#### 5. A Method of Simulating the Effect of Work Hardening

Consider the material whose stress-strain curve is given by Figure A-1a. Assume that  $\epsilon_c$ , the strain at the crack tip, is 8 per cent. For a given value of  $t$  (0.08 inch), the displacement at the crack tip can be calculated if it is assumed  $v_c = \frac{\epsilon_c t}{4} = 1.6 \times 10^{-3}$  in. For other points in the plastic zone, the displacement can be found from Figure 3 and the relation  $\epsilon/\epsilon_c = v/v_c$ . Since each strain will correspond to a flow stress on Figure A-1a, the tension-distance curve (Figure A-1b) can be calculated for a given  $T/Y$ . For ease in further computation, a two-step stress distribution, which simulates the calculated one is found by matching areas A and B (Figure A-1b) and the stress distribution in front of the plastic zone, the plastic-zone size, and displacements found by the method outlined in Section 4.

To determine the solid lines on Figure 6, the displacements ( $v_c$ ) corresponding to the various strains were calculated from Equations (11) and



(a) Engineering Stress-Strain Curve For the 3% Silicon Steel



(b) Tension - Distance Curve

FIGURE A-1. CONVERSION OF STRESS-STRAIN CURVE INTO TENSION-DISTANCE CURVE



(12) with  $t = 0.08$  inch. The two-step distribution was replaced by a uniform distribution and  $T/Y$  found from Figure 4. Although each solid line was calculated for a specific crack length and sheet thickness, it applies to any specimen with the same  $c/t$  ratio [see Equations (11) and (12) and (A-6)]. Plastic-zone sizes for 1/4-inch cracks in thicknesses other than 0.08 inch were found by determining  $c/t$  and interpolating between the curves of Figure 6.

### 6. Plastic-Zone Instability

If the applied stress is held constant, but the tension  $S$  (reflecting the yield stress of the material) is allowed to vary, the rate of change of the equilibrium zone size is given by

$$\left. \frac{\partial \ln \rho}{\partial \ln S} \right|_T = - \left( \sec \frac{\pi T}{2S} - 1 \right)^{-1} \left( \frac{\pi T}{2S} \sec \frac{\pi T}{2S} \tan \frac{\pi T}{2S} \right). \quad (\text{A-13})$$

It is necessary to postulate a variable  $S$  when we consider a zone loaded with non-uniform tension distribution,  $S(x)$ , which is to be represented by a uniform average tension  $\bar{S} = 1/\rho \int_c^{(c+\rho)} S \, dx$  (see Figure 5e). If the tension at the crack tip,  $S_c$ , changes, the corresponding change in plastic-zone size is easily seen to be

$$\frac{\partial \ln \rho}{\partial \ln \bar{S}} = \frac{-\bar{S}}{\bar{S} - S_c}. \quad (\text{A-14})$$

If the stress-strain curve is falling, i.e.,  $\frac{\partial S_c}{\partial \rho} < 0$ , and  $S_c < \bar{S}$ , the rate of increase in plastic-zone size predicted from Equation (A-13) may be larger than can be tolerated by the conditions of Equation (A-14). Thus an instability results when

$$\frac{\bar{S} - S_c}{\bar{S}} > \left( \sec \frac{\pi T}{2S} - 1 \right) \left( \frac{\pi T}{2S} \sec \frac{\pi T}{2S} \tan \frac{\pi T}{2S} \right)^{-1}. \quad (\text{A-15})$$

The crack-tip strain at plastic instability can be estimated by noting that the relation between  $Y'$  (true stress) and  $\epsilon^*$  (reduction in area) is approximately linear beyond the point of necking. Together with Equation (10), this leads to a simple parabolic relation between  $\epsilon^*$  and the tension  $S$  ( $S$  is equivalent to the engineering stress in a tensile test). The equation of the parabola with a vertex at  $U, \epsilon_u$ , and passing through  $F, \epsilon_f$  is

$$\epsilon^* = \epsilon_u + \sqrt{H \left( \frac{U-S}{U} \right)} \quad , \quad (A-16)$$

where  $H = \frac{U(\epsilon_f - \epsilon_u)^2}{(U - F)}$ , and  $U, \epsilon_u$ , and  $F, \epsilon_f$  are the engineering stress and strain at maximum load and fracture, respectively. The following approximation

$$\frac{\bar{S} - S}{\bar{S}} \approx \frac{U - S}{U} \quad (A-17)$$

is reasonable, particularly for high-strength materials exhibiting little work hardening. Consequently, the value of  $\epsilon_c^*$  corresponding to a critical value of  $\left( \frac{\bar{S} - S_c}{\bar{S}} \right)$  is

$$\epsilon_c^* \approx \epsilon_u + \sqrt{H \left( \frac{\bar{S} - S_c}{\bar{S}} \right)} \quad . \quad (A-18)$$

NATIONAL ACADEMY OF SCIENCES

Ship Hull Research Committee

Division of Engineering & Industrial Research

National Research Council

Chairman:

RADM A. G. Mumma, USN (Ret.)  
Executive Vice President  
Worthington Corp.

Members:

Mr. Hollinshead de Luce  
Assistant to Vice President  
Bethlehem Steel Co., Shipbuilding Div.

Dr. C. O. Dohrenwend  
Provost and Vice President  
Rensselaer Polytechnic Institute

Professor J. Harvey Evans  
Professor of Naval Architecture  
Massachusetts Institute of Technology

Mr. M. G. Forrest  
Vice President — Naval Architecture  
Gibbs & Cox, Inc.

Professor J. E. Goldberg  
School of Civil Engineering  
Purdue University

Mr. James Goodrich  
Executive Vice President  
Bath Iron Works

Mr. M. W. Lightner  
Vice President, Applied Research  
U. S. Steel Corporation

Arthur R. Lytle  
Director

R. W. Rumke  
Executive Secretary